Towards tunable defect arrangements in smectic liquid crystal shells utilizing the nematic-smectic transition in hybrid-aligned geometries†

Hsin-Ling Liang,[ab] Rudolf Zentel,[b] Per Rudquist,[c] and Jan Lagerwall*[ad]

Received Xth XXXXXXXXXX 20XX, Accepted Xth XXXXXXXXX 20XX
First published on the web Xth XXXXXXXXXX 200X
DOI: 10.1039/b000000x

We produce and investigate liquid crystal shells with hybrid alignment—planar at one boundary, homeotropic at the other—undergoing a transition between the nematic (N) and smectic-A (SmA) phases. The shells display a dynamic sequence of patterns, the details depending on the alignment agents and on the diameter and thickness of the shell. In shells of sufficient diameter we typically find a transient striped texture near the N-SmA transition, stabilising into a pattern of tiled, more or less regularly spaced focal conic domains in the SmA phase. The domain size and spacing decrease with reduced shell thickness. In case of strong homeotropic anchoring at one boundary and small shell size, however, the increased curvature favors homeotropic against planar alignment in the smectic phase, and the shell then tends to adapt complete homeotropic alignment at the final stage of the transition. This is the first study of hybrid-aligned smectic shells and the results constitute a beautiful demonstration of the capacity for dynamic structure formation and reformation via self-assembly in soft matter. The new patterns extend the range of arrays of topological defects that can be realised with liquid crystals in spherical morphology and the correlation between the feature arrangements and the variable parameters of the shell and its environment opens a route towards tunability. However, the observed strong impact from increasing curvature, even for these rather large shells, indicates that the choice of alignment agents inducing planar or homeotropic alignment with varying strength will become critical when targeting the most attractive colloidal size scale of about a micron or smaller.

1 Introduction

Liquid crystals (LCs) have been broadly studied in various configurations, most often in flat film morphology, leading to a highly prolific academic research fields as well as the immensily successful application in flat panel displays. An interesting recent development, very different from display applications where defects must be avoided at any price, is the research on well-controlled defect configurations and ways of applying them.[1–12] A fascinating special case is given by LC droplets[13,14] and shells[15,16] since the spherical topology in combination with planar alignment (director **n** in the plane of the drop/shell surface) ensures specific configurations of topological defects (disclinations) on the surface,[17] always with a net sum $s = 2$. The parameter s is the winding number that specifies how many full turns the director (or its projection on the surface) rotates around a defect. Such spherical LC structures were proposed for advanced colloidal applications,[18] as the tetrahedrally arranged defects expected in a planar-aligned nematic shell could anchor ligands in a quadrivalent configuration, opening for diamond colloidal crystal formation. Several other defect configurations are however possible and the possibility of achieving specific arrangements of defects in a controlled manner is thus a key point for applications.

Also smectic phases are attractive in this respect, as demonstrated so far in particular by Jung and co-workers,[3] who used lithographic channel substrates to produce periodic arrangements of smectic toroidal defects in which fluorescent microparticles can be trapped. The resulting well-ordered functional composites could be useful for new optoelectronic applications.[10] We recently presented the first study of defect configurations in planar-aligned LC shells undergoing a transition between nematic (N) and smectic-A (SmA) phases,[19] finding a dynamic behavior with formation of multiple charactistic patterns. These result from the frustration induced by the spherical shell morphology on the developing smectic phase

† Electronic Supplementary Information (ESI) available: movies ESI1 - ESI6 showing phase transitions of the shells discussed in the paper. See DOI: 10.1039/b000000x/

[a] *Institute of Chemistry - Physical Chemistry, Martin-Luther University Halle-Wittenberg, Von-Danckelmann-Platz 4, 06120 Halle, Germany.*
[b] *Institute of Organic Chemistry, Johannes Gutenberg University Mainz, Duesbergweg 10-14, 55099 Mainz, Germany.*
[c] *Chalmers University of Technology, Department for Microtechnology and Nanoscience, 412 69 Göteborg, Sweden.*
[d] *Graduate School of Convergence Science & Technology and Advanced Institutes of Convergence Technologies, Seoul National University, Suwon-si, Gyeonggi-do, Korea 443-270.*
Tel: +82 (0)31 888 9165; E-mail: jan.lagerwall@lcsoftmatter.com

in which the molecules organize in layers with constant thickness. Our results were largely corroborated by an independent and almost simultaneous study on the same system by Lopez-Leon *et al.*, coming to similar conclusions.[20]

In the present paper we vary the stabilizers (which simultaneously act as alignment agents) added to the aqueous inner and outer phases, thereby modifying the liquid crystal anchoring geometries and strengths at the two shell boundaries. Our focus is on hybrid alignment, where the inner interface ensures homeotropic alignment and the outer interface planar alignment, or vice versa. Upon inducing the N-SmA phase transition in these shells we find a series of compelling textural developments with an end result that can be quite different from the uniformly planar steady-state texture, typically with a more or less regular array of focal conic defects. The general texture type as well as the size of its features depend on shell size and thickness in addition to the choice of alignment agents in the internal and external phases, respectively.

2 Experimental section

2.1 Materials

A suspended LC shell system consists of three phases: the LC shell itself, an internal droplet of liquid that is immiscible with the liquid crystal, and an external liquid that must also be immiscible with the LC. The latter constitutes the continuous phase of the colloidal system whereas the two former together comprise the disperse phase. In this work, we use the smectogen 4-cyano-4-octylbiphenyl (8CB: SmA 33.5 N 41.5 Iso./°C; Synthon Chemicals) as the shell material, surrounded by different combinations of in- and outside aqueous solutions (Table 1). These generally contain glycerol, for raising the viscosity to values appropriate for the microfluidic shell production technique (described below) and at the same time yielding a density similar to that of the LC, in addition to a small amount of polymer or surfactant. The latter substances serve not only as interface stabilisers preventing shells from coalescence, but also as alignment agents inducing either planar or homeotropic anchoring of the LC director at the inner and outer shell boundaries. Poly(vinyl alcohol) (PVA; Acros Organics, Mw: 20,000-30,000, 88% hydrolysed) promotes planar alignment, sodium dodecyl sulphate (SDS; Roth, ultra pure grade) and sodium dodecyl benzene sulphonate (SDBS; Aldrich, technical grade) give homeotropic alignment, and the amphiphilic triblock copolymer Pluronic F127 (BASF) allows either orientation, with slight preference for homeotropic.[21]

2.2 Shell production

The LC shells are generated by flow focusing in an axisymmetric glass capillary microfluidic device.[22] Two tip-modified round capillaries with 1 mm outer diameter are counter-directionally nested into a square capillary with 1 mm inner dimension. One of the round capillaries serves as injection tube and is tapered by using a micropipette puller (Sutter Instruments P97, USA) to form a thin tip which is then cut to a desired orifice size of 20-40 μm diameter using a microforge (Narishige MF830, Japan). The opening of another capillary, the collection tube, is fire-polished to 80-200 μm inner diameter using a lighter or a hand torch. Fluid sources are connected to the capillary channel via a set of plastic tubings and fittings.

The interior phase is pumped through the injection tube, and then enwrapped by the 8CB flowing in the same direction through the square capillary, outside the injection tube. The exterior phase is pumped through the same square capillary from the other side, in the opposite direction. Since 8CB is immiscible with the surrounding phases, it forms a coaxial stream with the interior phase, which is then flow focused by the exterior phase into the collection tube, where it breaks up into a sequence of spherical shells due to the Rayleigh-Plateau instability (Fig. 1). The shell size and thickness are tuned by controlling the flow rates of the three fluids. In order to reduce the viscosity of 8CB during flow, the whole system is maintained at 60°C to have 8CB in its isotropic phase throughout the shell production process.

Table 1 List of 8CB shell systems with various pairs of non-identical alignment agents (P: planar, H: homeotropic) in the interior (*i*) and exterior (*e*) phases.

Label	Nematic alignment	Interior phase	Exterior phase
1	H*i*P*e*	SDS* (1 wt.-%)	PVA* (1 wt.-%)
2	P*i*H*e*	PVA* (1 wt.-%)	F127 (5 wt.-%)
3a	P*i*H*e*	PVA* (1 wt.-%)	SDBS* (1 wt.-%)
3b	P*i*H*e*	PVA* (1 wt.-%)	SDS* (1 wt.-%)

* These substances are dissolved in a mixture of water and glycerol (1:1 volume ratio).

2.3 Shell observation

The produced shells suspended in the exterior phase are collected through the collection tube into a petri dish, then filled into a flat capillary with an inner dimension larger than the di-

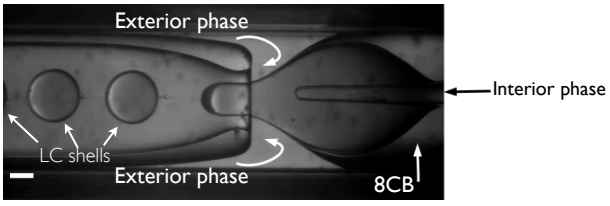

Fig. 1 8CB shell production in our microfluidic device, captured by a high speed camera. (Scale bar: 100 μm.)

ameter D of the shells. The flat capillary is placed onto a hot stage mounted on a polarising microscope with a video camera. In each observation session we heat and cool the shells between room temperature and 40°C for several times, recording videos throughout the process. This allows us to identify the key textural features at each stage.

The thickness $\bar{h}$ of the shells is measured in an optical microscope without polarisers. When adjusting the focal plane to the centre of the shell, the inner and outer boundaries can be clearly resolved, allowing an accurate measurement of the boundary distance for shells of the thicknesses considered in this paper. Although the inner droplet is not located exactly at the center position of the shell, due to imperfect density matching of the different fluids, the offset at top and bottom will be of equal magnitude but opposite sign, hence the measured mid-plane value is a good estimate for the average shell thickness $\bar{h}$. Moreover, since the ratio of shell thickness to radius is very small the thickness variation throughout the shell can be considered negligible to a first approximation.

3 Results and discussion

We investigate four sets of 8CB shells with different in- and exterior coupled confinement, all having one side planar and one homeotropic. The shells are somewhat thicker at the top than at the bottom due to the slightly higher densities of the interior aqueous solutions than that of 8CB.

3.1 Configuration 1: homeotropic interior, planar exterior

The interior phase of configuration 1 contains SDS, ensuring strong homeotropic, and thus defect-free, LC alignment at the inner shell boundary. In contrast, the PVA in the continuous phase imposes planar anchoring at the shell outside. Over this surface the director field must consequently have a total defect sum of $s = 2$. Within the hybrid nematic shell the director field connects the opposing boundary alignments continuously via a splay-bend deformation. In flat hybrid nematic films the projection of the average director onto the film surface is a two-dimensional unit vector field $\mathbf{c}(x,y)$ that is not sign invariant. Accordingly, $s = \pm 1/2$ disclinations in the $\mathbf{c}$-field are forbidden. Similarly, in hybrid nematic shells the projection of the average director onto the shell's outer surface is a vector field $\mathbf{c}(r,\phi,\theta)$, with r, ϕ and θ the radial, azimuthal and polar coordinates mapping the spherical surface, which in the same way excludes the formation of half-unit disclinations. The shell exterior must thus exhibit two $s = 1$ point defects in the $\mathbf{c}(r,\phi,\theta)$ director field and this is indeed what we see in the micrographs of the shell in its nematic state, shown in Fig. 2a-b and movie ESI1.

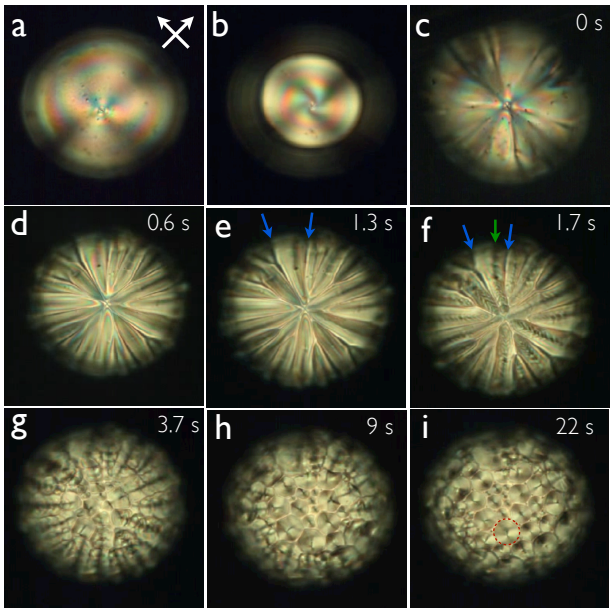

Fig. 2 N - SmA phase transition of an 8CB shell (D= 178 μm, $\bar{h}$= 14 μm) in configuration 1 (H*i*P*e*), observed in a crossed polarising microscope upon cooling at 2 K min.$^{-1}$ (stills from movie ESI1). In the N phase the planar outside exhibits two $s = 1$ surface point defects located at the shell top a) and bottom b), respectively. c)-d) Formation of striped texture at the shell top near the N - SmA phase transition. e)-f) The stripes are the edges of a corrugated nematic membrane. The blue arrows indicate the upper set of stripes, and the shadows (green arrow) in between are the lower set which is not in focus. g)-i) Formation of toroidal defects. g) Fish scale pattern formed from incomplete defect ellipses. i) The radius of the largest domain in view (red dashed circle) is $\approx$ 13 μm, corresponding to its depth which is about the shell thickness. Time indications refer to the time after the start of the phase transition.

For our planar-aligned outer shell boundary (as for the exterior of a freely suspended LC drop under planar confinement) there are two possible geometries for $\mathbf{c}(r,\phi,\theta)$, both giving the required two $s = 1$ point defects: in the *bipolar* geometry $\mathbf{c}$ extends along meridians from each defect point whereas it in the *concentric* geometry encircles each defect like the circles of latitude (parallels) on the earth, see e.g. Ref.[17]. The two geometries are topologically distinct but in regular polarising microscopy they appear texturally identical, with four extinction brushes around each defect point. One can however distinguish them by inserting a compensator plate in the polarising microscope, leading to color shifts that are in opposite directions for the two geometries. In this way we could confirm that our shells have the bipolar geometry, i.e. the director field on the shell's outer interface is directed meridionally around each defect.

If we draw the cross section of the shell in a plane containing both defects, as in Fig. 3, we see that the two defects

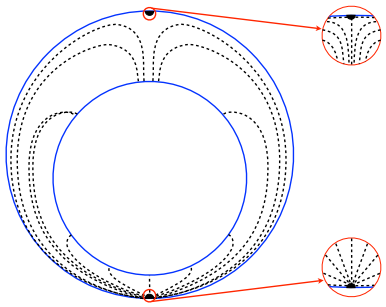

Fig. 3 Sketch of the 2D director field $\mathbf{n}_{cs}(r,\theta)$ (dashed lines) arising by making a flat cross section through a nematic H*i*P*e* shell. The cross section is chosen such that it contains both meridional $s=1$ defects in $\mathbf{c}(r,\phi,\theta)$ situated on opposite sides of the shell's planar-aligned outer surface. In the $\mathbf{n}_{cs}(r,\theta)$ field, these correspond to a half hyperbolic $s_{cs}=-1/2$ and a half radial $s_{cs}=+1/2$ defect, respectively, drawn in magnified scale in the red circles on the right.

differ in terms of the director field *within* the shell. For convenience we define the 2D director field of the cross section (*cs*) plane as $\mathbf{n}_{cs}(r,\theta)$. As for any plane without curvature, topology requires the defects as they appear in $\mathbf{n}_{cs}$ to fully cancel each other. In other words, within the cross section plane $\Sigma s_{cs}=0$, where we for clarity specifically define s_{cs} as the winding number in $\mathbf{n}_{cs}$. One of the defects is thus a half hyperbolic $s_{cs}=-1/2$ while the other is a half radial $s_{cs}=+1/2$ defect, cf. the magnified views on the right in Fig. 3. We have drawn the hyperbolic at the thicker and the radial at the thinner side of the shell, in agreement with the results of Lopez-Leon and Fernandez-Nieves from studying a gradual change from uniform planar to P*i*H*e* hybrid alignment.[23].

When the shell is cooled to the N - SmA transition temperature, a defect-free structure within the LC shell is no longer possible since the smectic organisation into equidistant layers is incompatible with director field bend. The resulting frustration phenomenon leads to a characteristic striped pattern sometimes referred to as 'oily streaks' or 'striations', which has been found in several previous studies of flat samples with antagonistic boundary conditions. We however note that the striped pattern can be classified into two types depending on if the striations are along[24] or perpendicular[25,26] to the projected **c** director field (further details will be discussed in a separate paper). As seen in Fig. 2c-f the stripes in our shells develop meridionally, i.e. along $\mathbf{c}(r,\phi,\theta)$, corresponding to the observations of stripes along $\mathbf{c}(x,y)$ in the flat hybrid samples studied by Cladis and Torza.[24] They found that the director bend is initially compressed to an increasingly thin layer within the sample bulk that remains in a nematic state due to a depression of the phase transition temperature induced by the bend distortion. In order to minimise the distortion this internal nematic layer buckles in alternating directions (Fig. 4a), extending the length over which the bend must take place. This yields the

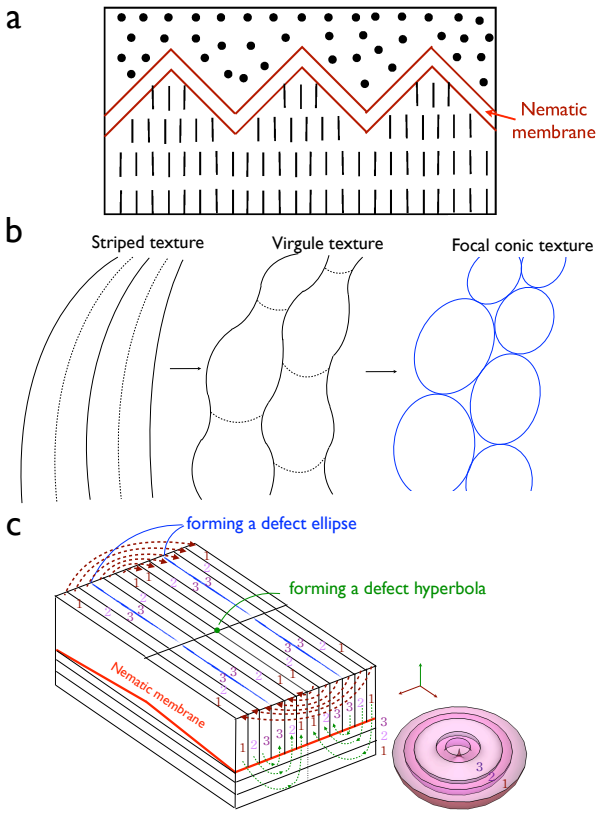

Fig. 4 Schematic illustration of the transformation from hybrid nematic to focal conic smectic organisation in the shell, following Cladis and Torza.[24]. (a) Sketch of a corrugated nematic membrane with compressed director bend connecting planar smectic layers at the top with homeotropic layers at the bottom at the onset of the N - SmA transition. (b) The transformation from striped to virgule to focal conic texture. (c) Schematic illustration of how smectic layers at the shell top and bottom curve in order to connect through focal conic domains. The first principle curvature is along the brown dashed arrows, the second is along the green dashed arrows.

characteristic texture with stripes along $\mathbf{c}(r,\phi,\theta)$.

As discussed by Cladis and Torza[24] the stripes are however not stable since the interfacial tension between nematic and smectic states triggers a Rayleigh-Plateau instability that rapidly breaks up the stripes (Fig. 4b). The smectic layers eventually eliminate the suppressed nematic membrane by curving such that they can connect to each other throughout the shell while still satisfying the opposing boundary conditions. The process first leads to a "virgule" texture[24] which then transforms into a focal conic texture once the curved layers have formed complete hemispherical domains. The details are illustrated schematically for the very simplified case of only a few smectic layers in Fig. 4c. In our shells the textural transformation takes place within a time frame of a few seconds, cf. Fig. 2f-i and movie ESI1. The hemispherical

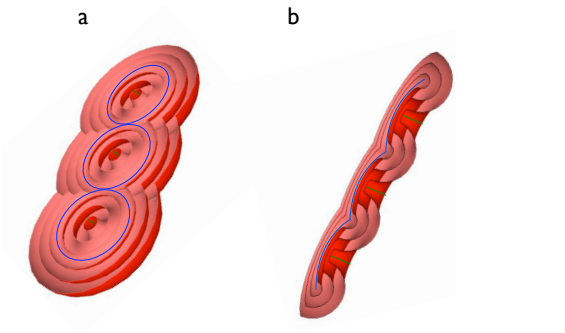

Fig. 5 a) Toroidal focal conic defects are composed of confocally bent smectic layers with defect circles (blue lines) and defect lines (green). In non-toroidal focal conics the defect lines bend into hyperbolae. Sketch b) is the side view of a).

domains that form the steady-state texture exhibit a toroidal focal conic organisation of the smectic layers (Fig. 4c., lower right).[7,27]

Since the smectic layer distance is fixed, the sizes of toroidal focal conic domains is limited by the sample thickness.[7] As illustrated in Fig. 5 the radius of any domain can be no greater than its depth, and thus no greater than the shell thickness in our case. We thus measure the largest toroidal domain in view (Fig. 2i, red dashed circle), obtaining a radius of about 13 μm which matches the average shell thickness very well. In a thinner shell the maximum lateral size of the toroidal defects must be smaller, and this is exactly what we find. Fig. 6 and movie ESI2 show the texture sequence observed during the N-SmA transition in an 8CB shell with the same H*i*P*e* configuration 1, SDS in the inner aqueous phase and PVA in the continuous phase, but the shell is here only 6 μm thick. The textural development is qualitatively similar to that of the thicker shell but the final pattern has much smaller domains. The maximum domain radius is now about 6 μm, equal to the shell thickness, as expected.

Finally, in this thinner shell it is also striking that at the onset of the N-SmA transition the effective birefringence Δn suddenly increases, the purple center turning orange-yellow. The same phenomenon most likely occurs in the thicker shell but as the total optical path difference (both the top and the bottom sides of a shell contribute) is here so large, reaching the fourth or even fifth order of the Michel-Levy diagram, a change in Δn has a much less visible effect. We believe that the origin of this increase is an increasingly uniform director field across the complete shell exterior, approaching straight north-south meridians like on the earth. The micrographs focusing on the shell top and bottom in the nematic phase in Fig. 6a and b reveal slightly different brush orientations, indicating that fluctuations in the nematic director field throughout the shell render the projections of **n** at the shell top and bottom, respectively, non-coplanar, reducing the effective birefringence. As the transition to smectic order is approached the expulsion of director bend straightens up the director field, resulting in a fully constructive addition of the birefringence from the top and bottom surfaces, explaining the change in colour.

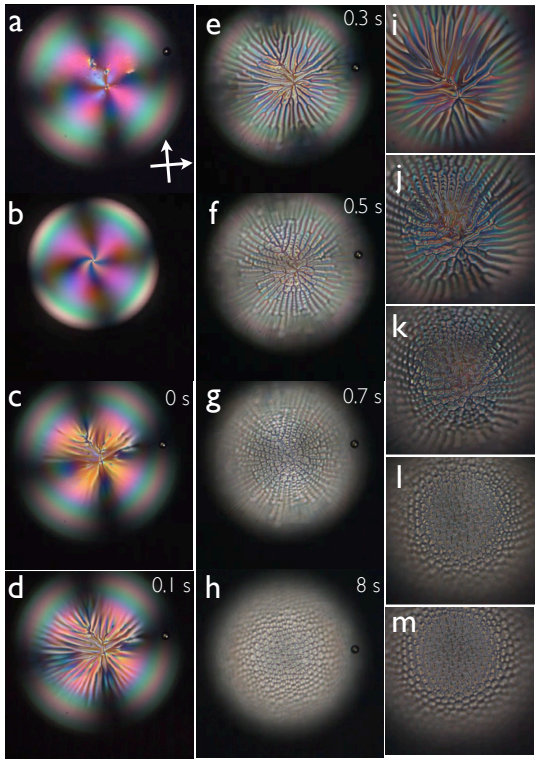

Fig. 6 N - SmA transition of a thin ($\bar{h}$= 6 μm, D= 350 μm) configuration 1 (H*i*P*e*) shell, observed in a crossed polarizing microscope on cooling at 2 K min.$^{-1}$ (stills from movie ESI2). Two s = 1 point defects located on the top a) and bottom b) outer surface in the N phase. c)-d) Formation of striped texture. f)-h) Development of toroidal defects, twice magnified in i)-m). The radius of the largest toroidal domain in view is $\approx$ 6 μm, similar to $\bar{h}$. Time indications refer to time after the start of the transition.

3.2 Configuration 2: planar interior, weak homeotropic exterior

In configuration 2 the shell is under PVA (interior) - F127 (exterior) confinement. As mentioned above F127 gives only a weak preference for homeotropic alignment but because the shell is relatively thick (13-14 μm) and since PVA acts only on the interior boundary, which is smaller than the exterior one, F127 succeeds in imposing homeotropic 8CB anchoring at the shell exterior. We thus again obtain a hybrid alignment but this time the geometry is reversed to P*i*H*e* type. The impact of this reversal on the textural development during the N - SmA phase transition is relatively small. The configuration

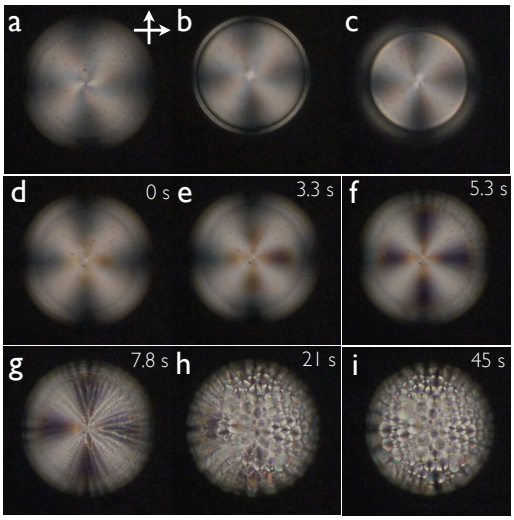

Fig. 7 N - SmA transition in a configuration 2 shell (P*i*H*e*, D = 200 μm , $\bar{h}$= 13-14 μm), observed in a crossed polarising microscope on cooling at 1 K min.$^{-1}$ (stills from movie ESI3). Two s = 1 point defects are seen on the top a) and bottom c) surface in the N phase. The shell boundaries are clearly seen in b), focused at the shell mid plane. d)-f) Colours appear in the extinction cross near the N - SmA phase transition. g)-i) Formation of stripes and toroidal defects. In this case, the defect ellipses should form at the inner surface, and at the outer surface there should be toroidal defect indentations. Time indications refer to the time after the start of the phase transition.

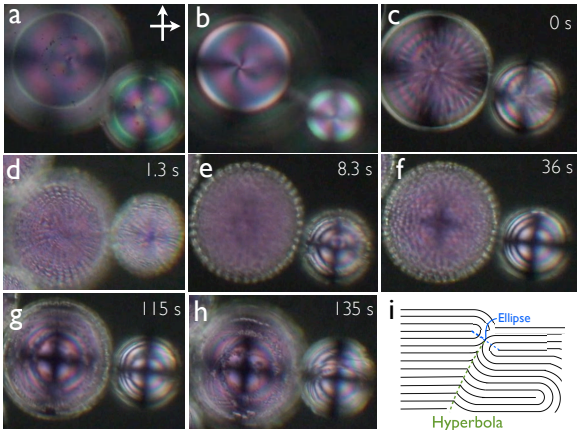

Fig. 8 N - SmA phase transition of configuration 3 shells (P*i*H*e* in the N phase; D= 220 and 145 μm, respectively; $\bar{h}$= 8-9 μm), observed in crossed polarising microscope on cooling at 1 K min.$^{-1}$ (stills from movie ESI4). Point defects (s = 1) at the top a) and bottom b) inner surfaces in the N phase. c) Formation of stripes in the SmA phase, and d) focal conic defects. e) The small shell changes to H*i*H*e* geometry, the large remains tiled with focal conics. f) A Maltese cross emerges in the larger shell, concurrent with shrinking and vanishing of focal conics. g)-h) The transition ends with H*i*H*e* geometry also in the large shell, with a few remaining focal conics stabilized at smectic layer steps. i) Sketch of smectic layer steps forming focal conic defects with adjacent plateaus.[28] Time indications refer to time after the start of the phase transition.

2 shell investigated, which has similar dimensions to that in Fig. 2, reveals qualitatively identical textural phenomena during the process, involving stripes as transitory and focal conic domains as final texture, cf. Fig. 7 and movie ESI3. Here we can also see clear signs of the straightening of the director field at the onset of the phase transition. In the nematic phase the center of the Maltese extinction cross is absent or distorted (panes a-c), revealing that the director field is non-coplanar at the shell top and bottom. As bend deformations are expelled upon approaching the SmA phase the director field is homogenized, and as a result the cross straightens and extends all the way to the center when the phase transition starts, where it however becomes distinctly colored. This is typical for a director field with light twist along the viewing direction, and it reveals that the straightening of the meridians is not complete.

A difference to the configuration 1 shells is that the focal conic domains here should have the defect ellipses at the inner, planar-aligned, boundary, and indentations coincident with the defect lines at the outer surface. Note that the defect line in each focal conic domain is distinctly off-centre, in contrast to the configuration 1 shell where all domains have a spot very close to the centre, corresponding to the defect line along the viewing direction. In contrast, the hyperbolae are apparently not fully degenerated into straight radially directed lines in the configuration 2 shell in Fig. 7. Rather than being a consequence of the reversal of the geometry (H*i*P*e* $\rightarrow$ P*i*H*e*) it is probably more likely due to the weaker homeotropic anchoring of F127 compared to SDS.

3.3 Configuration 3a: planar interior, moderately strong homeotropic exterior

We retain the P*i*H*e* geometry but exchange the weak homeotropic-aligning agent F127 in the continuous phase for the surfactant SDBS, giving a substantially stronger homeotropic anchoring at the shell exterior. The shell interior still contains PVA for planar alignment, in addition to a small amount of red dye that was here added for better distinguishing the internal droplet. This gives the shells a pinkish background color, as seen in Fig. 8 and 9 and movies ESI4 and ESI5. The director geometry in the nematic phase (Fig. 8a-b) again comprises a bend, connecting the planar inside to the homeotropic outside. The transition to SmA starts similarly to the previous hybrid shells, with meridional stripes rapidly breaking up into a defect-rich focal conic tiling pattern (c-d).

However, the stronger homeotropic anchoring on the outside now renders this an unstable state and the shells undergo yet another rearrangement of the internal structure shortly af-

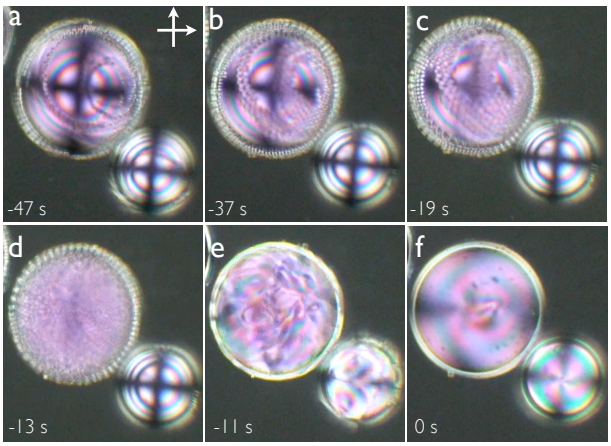

Fig. 9 SmA - N phase transition of the same shells as in Fig. 8, now followed on heating at 1 K min.$^{-1}$ starting with H*i*H*e* geometry (stills from movie ESI5). a)-c) Growth of necklaces of focal conics at smectic layer steps near the transition to the N phase. d) Focal conic defects completely cover the surface of the large shell, followed by the loss of smectic order in (e). f) Shells are back to P*i*H*e* hybrid alignment in the N phase. The small shell stays in the defect-free homeotropic alignment throughout the smectic phase, generating no focal conic domains at any time. Time indications refer to the time before the development of the steady-state nematic texture.

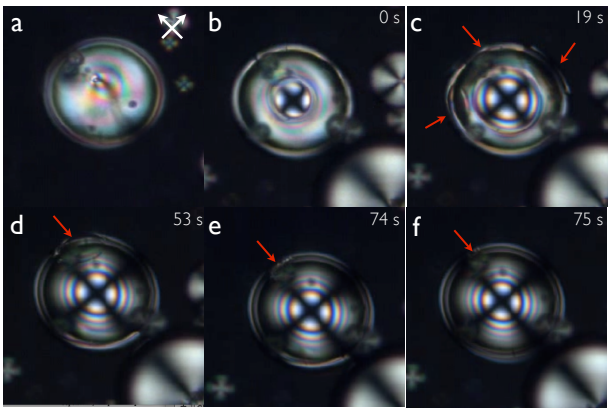

Fig. 10 N - SmA phase transition of configuration 3b shell (initial P*i*H*e* nematic alignment, D= 135 μm, $\bar{h}$= 6 μm), observed in a crossed polarizing microscope upon cooling at 1 K min.$^{-1}$ (stills from movie ESI6). a) One of the two s = 1 point defects in the N phase at the top inner surface. b) The fully homeotropic (H*i*H*e*) SmA phase appears as a circle with growing radius. c)-f) Other circles with H*i*H*e* SmA phase appear (red arrows), and finally merge together into a fully homeotropic smectic shell. Time indications refer to time after the start of the phase transition.

ter the transition (Fig. 8e-f). The focal conic domains shrink and eventually vanish, concurrent with the occurrence of uniform homeotropic alignment (H*i*H*e*) with birefringence rings and a Maltese cross. At the very end, in the stable SmA phase, the shells have transformed almost completely to homeotropic alignment (Fig. 8g-h). The time required for this alignment transformation decreases with shell size. In a small shell the stronger curvature increases the frustration encountered by a (partially) planar-aligned smectic phase [19], hence the tendency to leave planar alignment is enhanced. Consequently, large shells retain the P*i*H*e* hybrid alignment with focal conics substantially longer than small shells, which almost immediately after the transition turn completely homeotropic, cf. Fig. 8e-h.

Some time after reaching the smectic state only a few remaining focal conic domains can be seen at smectic layer steps (schematically drawn in Fig. 8i), similar to observations on stepped drops where strings of focal conics are often found along layer steps. [28,29] These strings of focal conic 'pearls' are more clearly seen in the photos in Fig. 9a-c, taken during a re-heating process on the same shells as in Fig. 8. As the sample approaches the nematic phase (Fig. 9b-d) it is apparent that the focal conic domains in the larger shell start to multiply originating from the strings, and just before the phase transition they again tile the whole shell. The shells then lose their positional order as they enter the nematic phase, turning back to P*i*H*e* hybrid alignment with two topological point defects. Note that the small shell retains the fully homeotropic alignment throughout the heating process, until the very phase transition, at which it abruptly changes to hybrid alignment without forming the transient focal conic tiling.

3.4 Configuration 3b: planar interior, strong homeotropic exterior; small and thin shell

Similar to configuration 3a, the shell in configuration 3b is also under competitive opposing anchoring conditions generating P*i*H*e* hybrid alignment in the N phase, but the surfactant in the continuous phase is this time SDS. Because technical grade SDBS contains not only linear but also branched isomers, the higher purity of the SDS sample may be expected to give slightly stronger homeotropic alignment. Moreover, the dominance of the hometropic alignment is further enhanced by reducing the shell size further.

As usual the shell exhibits hybrid alignment with two point defects in the N phase, cf. Fig. 10a, but it directly transforms to complete homeotropic alignment at the transition to SmA (b-f), instead of via stripes and focal conic domain tiling as in the previous samples. As is best seen in the movie ESI6, the H*i*H*e*-aligned smectic phase enters as circular domains that grow radially until they meet another domain at which point they merge. The first homeotropic-aligned domains nucleate at the defects but soon several other domains appear (indicated by red arrows in Fig. 10), growing also from initially defect-free regimes.

4 Conclusions and outlook

By preparing shells of the liquid crystal 8CB with various diameters and thicknesses, and with different stabilizers added to the internal and external aqueous phases inducing hybrid geometries we can generate a variety of transitory as well as stable textures as the shell transitions between the nematic and smectic-A phases. The high-temperature N phase exhibits two $s = 1$ point defects at the lowest and highest points of the shell and as the transition to SmA takes place a striped pattern typically grows out meridionally from each defect. This reflects a zigzag-shaped membrane of persisting nematic phase that temporarily separates the homeotropic and planar interfaces. A Rayleigh instability quickly destabilises the striped pattern, however, and the shell instead takes on an internal structure characterized by a tiling of more or less toroidal focal conic domains. The radius of the domain must be equal to its depth, which is restricted by the shell thickness, hence the radii of the largest focal conics in our sample are equal to the shell thickness. If the shell thickness is reduced the size of the domains diminishes accordingly. By changing the shell thickness we can thus tune the number of defects and periodicity of the generated pattern, giving us a control handle that may be attractive for new applications in liquid crystal-based colloids. The result is largely the same for both cases of hybrid alignment, planar on inside and homeotropic on outside, or vice versa.

If in a hybrid shell the homeotropic alignment dominates over the planar on the opposite side, the focal conic tiling can be rendered unstable, and the originally planar-aligned side transforms into homeotropic alignment in the SmA phase. The smaller and thinner the shell, the more rapidly it completes this alignment transformation, and in the extreme case the shell does not generate the toroidal tiling at all but transforms directly between hybrid N alignment and a fully homeotropic SmA phase. In order to maintain the focal conic domain tiling of hybrid shells also in very small shells, one may thus need a stronger planar-aligning agent than PVA, and it may be wise to use weak homeotropic-aligning agents such as F127 for the other interface.

The study of liquid crystal ordering in shell geometry constitutes a fascinating field of soft matter physics, providing an excellent example of strong response to very subtle modifications of the system conditions, but it also holds potential for applications. As our understanding develops of which defect structures can be formed in the shells, and how we can tune them by varying the geometrical features and/or the chemical environment at the two shell boundaries, we are building up a versatile toolbox for creating advanced colloids that may self-assemble into complex superstructures thanks to additives anchored in the regularly arranged defects. Combining this study with previous investigations on strictly nematic or strictly planar-aligned shells it is clear that we can generate anything from zero to a very large number of regularly spaced defects using even very simple liquid crystal phases like 8CB, and by changing the temperature we can dynamically modulate the configuration. It will be an important study field for the future to investigate the interaction between e.g. nanoparticles or biohybrid molecules with the defects in the shells.

Acknowledgements

This work is supported by the German Academic Exchange Service, the "Excellenzcluster nanostrukturierte Materialien" (Sachsen-Anhalt, Germany), International Research Training Group 1404 (IRTG University Mainz), the Advanced Institutes of Convergence Technology (SNU, Korea) grant nr. 490-20100024, and the National Research Foundation (Korea) grant nr. 490-20110016. We thank S. Schymura for valuable discussions, E. Fleischmann and R. Rix for help with the experimental set-up at University of Mainz and Y.-T. Tu for support with graphical design.

References

1 J. H. Kim, Y. H. Kim, H. S. Jeong, E. K. Youn and H.-T. Jung, *J. Mater. Chem.*, 2011, **21**, 18381–18385.
2 F. Serra, K. Vishnubhatla, M. Buscaglia, R. Cerbino, R. Osellame, G. Cerullo and T. Bellini, *Soft Matter*, 2011, **7**, 10945–10950.
3 Y. Kim, D. Yoon, H. Jeong, O. Lavrentovich and H. Jung, *Adv. Funct. Mater.*, 2011, **21**, 610–627.
4 U. Tkalec, M. Ravnik, S. Copar, S. Zumer and I. Musevic, *Science*, 2011, **333**, 62–65.
5 U. Tkalec, M. Ravnik, S. Zumer and I. Musevic, *Phys. Rev. Lett.*, 2009, **103**, 127801.
6 W. Guo and C. Bahr, *Phys. Rev. E*, 2009, **79**, 011707.
7 W. Guo and C. Bahr, *Phys. Rev. E*, 2009, **79**, 061701.
8 W. Guo, S. Herminghaus and C. Bahr, *Langmuir*, 2008, **24**, 8174–8180.
9 C. Bohley and R. Stannarius, *Soft Matter*, 2008, **4**, 683–702.
10 D. Yoon, M. Choi, Y. Kim, M. Kim, O. Lavrentovich and H. Jung, *Nat. Mater.*, 2007, **6**, 866–870.
11 A. Eremin, C. Bohley and R. Stannarius, *Phys. Rev. E*, 2006, **74**, 040701.
12 M. Choi, T. Pfohl, Z. Wen, Y. Li, M. Kim, J. Israelachvili and C. Safinya, *Proc. Natl. Acad. Sci. USA*, 2004, **101**, 17340–17344.
13 G. J. Koenig, I. Lin and N. Abbott, *Proc. Natl. Acad. Sci. U. S. A.*, 2010, **107**, 3998–4003.
14 J. Loudet, H. Richard, G. Sigaud and P. Poulin, *Langmuir*, 2000, **16**, 6724–6730.
15 T. Lopez-Leon, V. Koning, K. B. S. Devaiah, V. Vitelli and A. Fernandez-Nieves, *Nat. Phys.*, 2011, **7**, 391–394.
16 M. Bates, G. Skacej and C. Zannoni, *Soft Matter*, 2010, **6**, 655–663.
17 T. Lopez-Leon and A. Fernandez-Nieves, *Colloid Polym. Sci.*, 2011, **289**, 345–359.
18 D. Nelson, *Nano. Lett.*, 2002, **2**, 1125–1129.
19 H.-L. Liang, S. Schymura, P. Rudquist and J. Lagerwall, *Phys. Rev. Lett.*, 2011, **106**, 247801.
20 T. Lopez-Leon, A. Fernandez-Nieves, M. Nobili and C. Blanc, *Phys. Rev. Lett.*, 2011, **106**, 247802.
21 H.-L. Liang, E. Enz, G. Scalia and J. Lagerwall, *Mol. Cryst. Liq. Cryst.*, 2011, **549**, 69–77.

22 A. Utada, E. Lorenceau, D. R. Link, P. D. Kaplan, H. A. Stone and D. A. Weitz, *Science*, 2005, **308**, 537–541.
23 T. Lopez-Leon and A. Fernandez-Nieves, *Phys. Rev. E*, 2009, **79**, 021707.
24 P. Cladis and S. Torza, *J. Appl. Phys.*, 1975, **46**, 584–599.
25 E. Lacaze, J.-P. Michel, M. Alba and M. Goldmann, *Phys. Rev. E*, 2007, **76**,.
26 B. Zappone and E. Lacaze, *Phys. Rev. E*, 2008, **78**,.
27 O. Pishnyak, Y. Nastishin and O. Lavrentovich, *Phys. Rev. Lett.*, 2004, **93**, ARTN 109401.
28 D. Demus, *Textures of liquid crystals*, Verlag Chemie, Weinheim, 1978.
29 Y. Bouligand, *Journal de Physique*, 1972, **33**, 525–547.